Multicritical behaviour of $Fe_{0.5}Ni_{0.5}Cl_2$, a Heisenberg antiferromagnet with intermediate uniaxial anisotropy

1990 J. Phys.: Condens. Matter 2 4495

(http://iopscience.iop.org/0953-8984/2/19/015)

J. Phys.: Condens. Matter 2 (1990) 4495–4505. Printed in the UK

Multicritical behaviour of $Fe_{0.5}Ni_{0.5}Cl_2$, a Heisenberg antiferromagnet with intermediate uniaxial anisotropy

B Igel†, W Kleemann† and I Vilfan‡

† Angewandte Physik, Universität Duisburg, D-4100 Duisburg, Federal Republic of Germany

‡ J Stefan Institute, YU-61111 Ljubljana, Yugoslavia

Received 16 October 1989

Abstract. First-order phase transitions are induced by an axial magnetic field in the disordered antiferromagnet $Fe_{0.5}Ni_{0.5}Cl_2$ ($T_N = 40.9$ K) below the tricritical point ($H = 2.97$ T, $T = 29.3$ K). The thermodynamic first-order transition line separates the antiferromagnetic (AF) from the paramagnetic (PM) phase down to a critical end point ($H = 3.40$ T, $T = 19.3$ K), below which AF-to-spin-flop (SF) transitions are found. Second-order SF-to-PM transitions occur at slightly higher fields. This is the first experimental evidence of the unusual multicritical behaviour of Heisenberg antiferromagnets with intermediate uniaxial anisotropy as predicted by Vilfan and Galam. Magnetic phase diagrams calculated using realistic exchange and anisotropy model parameters in the virtual-crystal approximation are in qualitative agreement with the experimental data obtained from Faraday rotation measurements.

1. Introduction

Multicritical behaviour has been investigated very extensively for antiferromagnets with uniaxial anisotropy, which are exposed to an external magnetic field H along the easy axis [1–3]. Special interest has been focused on the experimentally available extreme cases of both strong and weak anisotropy. For strong anisotropies, a first-order phase boundary separating the antiferromagnetic (AF) from the paramagnetic (PM) phase may arise in the H versus T phase diagram at low temperatures T, ending at a tricritical point (TCP) (H_t, T_t) [4]. The phase line between the TCP and the Néel point ($H = 0$, $T = T_N$) is characterised by second-order phase transitions. In the opposite extreme, for weak anisotropies, at low temperatures a spin-flop (SF) phase is expected to separate the PM from the AF phase up to the bicritical point (BCP) (H_b, T_b) [5].

Excellent experimental evidence for both limiting cases has been achieved for a number of model materials. For example $GdAlO_3$ proves to be prototypic for SF behaviour [2], whereas $Dy_3Al_5O_{12}$ [3] and $FeCl_2$ [6] are well known for their low-T metamagnetic spin-flip behaviour which can be observed up to the well defined TCP. On the other hand, systems with intermediate uniaxial anisotropy are relatively rare. In this respect, theory is much more advanced. A rich variety of very different H versus T phase diagrams with additional critical end points (CEPs) [7] and new multicritical points (NMPs) [8] has been deduced but not yet been verified experimentally up to now. The NMP scenario was first detected by Galam and Aharony [9] as the coalescence of a BCP and a TCP occurring in an anisotropic ferromagnet in a random longitudinal field. Vilfan

0953-8984/90/194495 + 11 $03.50

and Galam [8] confirmed its existence in a spin-1 Heisenberg antiferromagnet with ferromagnetic next-nearest-neighbour interaction and intermediate uniaxial anisotropy. The experimental verification of systems with intermediate anisotropies was suggested [8] to be achievable by alloying systems with appropriate extreme uniaxial anisotropies and intermediate mixing ratios.

Systematic experimental studies of mixed anisotropy systems in external magnetic fields were performed and reported in [10], where mixtures of uniaxial (Ising-like) $FeCl_2$ and isostructural planar (xy-like) $CoCl_2$ were investigated. At $H = 0$, the mixed system $Fe_{1-x}Co_xCl_2$ orders uniaxially along the crystallographic c direction at low T for small x ($\leqslant 0.3$) and in a planar manner (in the c plane) for large x. Whereas pure $FeCl_2$ is a strongly anisotropic metamagnet, the mixed systems ($0 < x \leqslant 0.3$) have a smaller anisotropy on the average. Therefore a SF phase should appear at low temperatures and high fields. Indeed, the SF phase was observed [10] in samples with $x = 0.275$ and 0.286. Later, Nitsche and Kleemann [11] found evidence for the predicted [8] crossover from the strong- to the weak-anisotropy case. Whereas an $x = 0.20$ sample is metamagnetic like pure $FeCl_2$ [6] with a TCP at (0.83 T, 13.9 K), a sample with $x = 0.27$ reveals a SF phase at all temperatures up to the BCP (0.15 T, 14.6 K). Samples with intermediate concentrations ($0.20 < x < 0.27$) have not yet been investigated. They are expected [8, 9] to reveal the gradual growth of a low-T SF phase, terminated by a CEP, which eventually merges into the TCP at some critical concentration.

In the present paper a part of this unusual scenario is evidenced on a related system, $Fe_{0.5}Ni_{0.5}Cl_2$. In this mixture of Ising-like $FeCl_2$ with $NiCl_2$, a compound with weak xy anisotropy, the regime with longitudinal AF spin order ($S = 1$) is fairly broad, $0 \leqslant x \leqslant 0.88$ [12]. Hence, the intermediate anisotropy range, lying between the metamagnetic ($x = 0$ [6]) and SF ($x = 0.85$ [12]) extremes, should be easier to locate than in $Fe_{1-x}Co_xCl_2$. Our data for $x = 0.5$ show, for the first time, the appearance of a CEP, in which the first-order phase boundary between the AF and the SF phase at low T coincides with the first-order boundary between the AF and the PM phases at intermediate temperatures. Model calculations with realistic system parameters along the lines previously described [8] are shown to be in qualitative agreement with the experimental phase diagram.

2. Experimental procedure

Single crystals of $Fe_{0.5}Ni_{0.5}Cl_2$ were grown by the Bridgman technique from equimolar mixtures of the anhydrous pure compounds $FeCl_2$ and $NiCl_2$. The actual concentration is estimated to be correct within errors Δx of ± 0.05. This follows from a comparison of the measured zero-field Néel temperature T_N of 40.9 K, with the T versus x phase diagram reported by Ito *et al* [13].

The sample used in this investigation was cleaved from the bulk crystal, shaped to an approximately circular disk with a diameter of 3.9 mm and a thickness of 0.57 mm along the rhombohedral c axis. A thin coating of paraffin was finally used in order to protect the slightly hygroscopic sample from surface deterioration by moisture and to stick it to the sample holder.

The magnetisation has been determined as a function of both T and H ($\boldsymbol{H} \| \boldsymbol{c}$) by measuring the magneto-optical Faraday rotation (FR) θ. This quantity is expected to be strictly proportional to M, since this applies to both limiting cases, $FeCl_2$ [6] and $NiCl_2$ [14]. Experimental details concerning the optical and cryogenic techniques involved

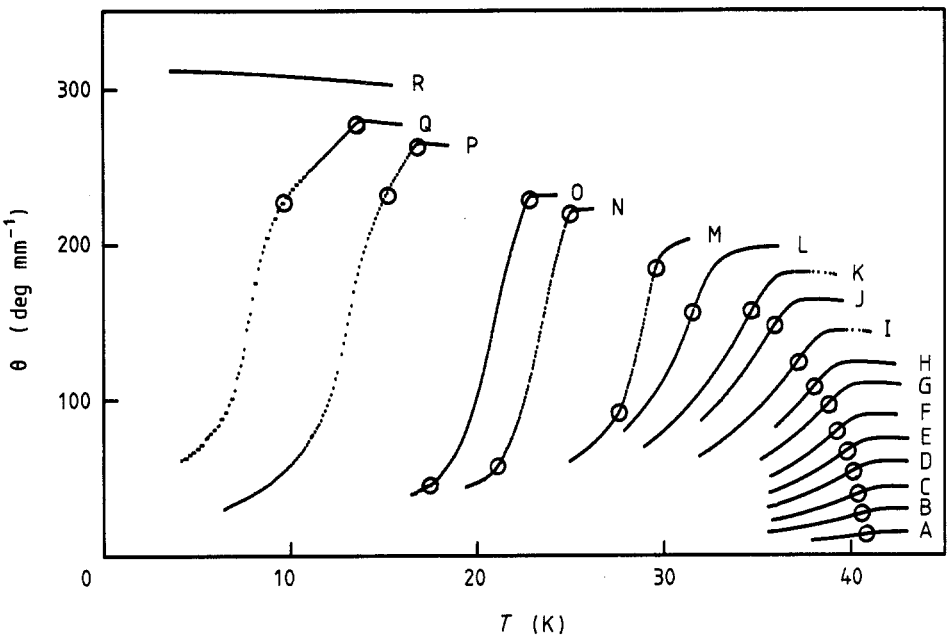

Figure 1. Specific Faraday rotation θ of $Fe_{0.5}Ni_{0.5}Cl_2$ measured with light of $\lambda = 633$ nm at fixed applied fields $H_a = 0.25$ T (curve A), 0.49 T (curve B), 0.73 T (curve C), 0.98 T (curve D), 1.23 T (curve E), 1.48 T (curve F), 1.74 T (curve G), 1.97 T (curve H), 2.24 T (curve I), 2.53 T (curve J), 2.74 T (curve K), 2.96 T (curve L), 3.11 T (curve M), 3.36 T (curve N), 3.46 T (curve O), 3.74 T (curve P), 3.86 T (curve Q); 4.11 T (curve R) as a function of the temperature. The phase transition points are indicated by open circles (see text).

were given in [11]. In particular, reliable FR data require the absence of in-plane birefringence due to internal strains, which has carefully been ascertained with the help of a polarising microscope. He–Ne laser light at $\lambda = 633$ nm proves to be most appropriate for the FR measurements because of an absorption minimum of $Fe_{0.5}Ni_{0.5}Cl_2$ in that spectral range.

3. Experimental results

Figure 1 shows the FR θ versus T, measured at various fixed values of the applied field in the range $0.25\ \text{T} \leqslant H_a \leqslant 4.11\ \text{T}$. As was argued in our previous investigations of the FR of $FeCl_2$-like mixed systems, $Fe_{1-x}Co_xCl_2$ [11] and $Fe_{1-x}Mg_xCl_2$ [15], the phase transition temperatures are readily determined from points of inflection and bending points. As indicated by the open circles on curves A–L in figure 1, second-order phase transitions do occur in the low-field regime $H_a \leqslant 3$ T. As expected [11, 15], in that range the crossover from random-exchange Ising model (REIM) to RF Ising model (RFIM) critical behaviour takes place. It is characterised by a gradual change in the asymmetric $(\partial M/\partial T)_H$ versus T curve into a symmetric logarithmic divergence on increasing H. This is compatible with a RFIM specific heat exponent $\tilde{\alpha} = 0$ [16]. The variation $T_c(H)$ versus H yields a crossover exponent $\Phi = 1.48 \pm 0.01$ in close agreement with the widely accepted

value $\Phi = 1.42 \pm 0.02$ [15]. Details of these and other RF properties of $Fe_{0.5}Ni_{0.5}Cl_2$ in the low-H limit are discussed elsewhere [17].

Here we are primarily interested in the occurrence of first-order phase transitions in the higher-field range. Indeed, the expected AF-to-PM transition is clearly indicated by two successive bending points as shown for $3.11\ T \leqslant H_a \leqslant 3.46\ T$ in curves M–O in figure 1. They are connected by essentially linear θ versus T curves, which are typical of the mixed AF–PM domain phase [6, 18]. This characterises the metamagnetic phase transition whenever experiments are done in a constant applied field H_a on a sample with non-vanishing demagnetisation factor N. This typical signature changes, however, at somewhat larger field values. As shown by curves P and Q in figure 1 ($H_a = 3.74$ T and 3.86 T, respectively) an additional bending point, albeit slightly smeared, is clearly observed at intermediate temperatures, whereas the low-T (or low-θ) bending points are not clearly marked (omitted in curves P and Q). In the low-T range the θ versus T curves are again as steep as in the metamagnetic regime (curves M–O), but they flatten appreciably above the new bending point and below the well defined paramagnetically saturated regime. Here, for the first time the signature of an additional phase transition into an intermediate SF phase becomes apparent. Clearly, its range of existence decreases on raising the temperature (or lowering H_a). Finally, at large enough fields (figure 1, curve R) the PM phase is induced at all temperatures.

The data in figure 1 will be used below to construct part of the H_a versus T phase diagram. Obviously, however, this seems to be rather flat in the most interesting range, $3.4\ T \leqslant H \leqslant 4.0\ T$. In that region, better resolved data are available from isothermal θ versus H_a scans, i.e. on paths nearly orthogonal to the H_a versus T phase boundary. The resulting magnetisation curves obtained at various temperatures in the range $5\ K \leqslant T \leqslant 40\ K$ in fields up to $H_a = 4.5\ T$ are shown in figure 2. The REIM-to-RFIM crossover range is represented by curves A–C ($40\ K \geqslant T \geqslant 30.5\ K$). It is, again, characterised by only one point of inflection at $H_{ac}(T)$ (open circles in figure 2). In the metamagnetic regime, steep linearly varying θ versus H_a curves terminated by well defined bending points $H_{ac}^{-}(T)$ and $H_{ac}^{+}(T)$ do arise, as usual [11] (curves D–F in the temperature range $27.5\ K \geqslant T \geqslant 22.7\ K$). In the very-low-$T$ range ($18.7\ K \geqslant T \geqslant 5\ K$), θ versus H_a reveals a novel linear part with intermediate slope between H_{ac}^{+} and the sharp bending point at the PM phase boundary H_{ac}'. We believe this extra part of the magnetisation curve to be due to the above-conjectured SF phase. Its range of existence clearly shrinks as temperature increases, but the true position of H_{ac}^{+} is difficult to determine because of increasing rounding. In order to determine the CEP as the locus, where the SF phase just vanishes, it proves useful to inspect the derivative curves of $d\theta/dH_a$ versus H_a. Apart from a central, roughly symmetrical peak extending from H_{ac}^{-} to H_{ac}^{+}, one finds a shoulder due to the SF phase within H_{ac}^{+} and H_{ac}'. By graphical decomposition of various magnetisation curves, recorded at 0.5 K intervals in the range $18\ K \leqslant T \leqslant 22\ K$, we eventually find that the shoulder vanishes at $H_{a,CEP} = 3.62 \pm 0.05$ T and $T_{CEP} = 19.3 \pm 0.3$ K.

Before discussing the way to construct further elements of the phase diagram from the above data, we notice that the lower part of the θ versus H_a transition curve ($H_{ac}^{-} \leqslant H_a \leqslant H_{ac}^{+}$), does not preserve its linearity (cf curves E and F) upon cooling to below about 20 K (curves G–J). Instead, it becomes rounded with a variable slope between these field limits, preserving its near-tricritical value only on the average. The reasons for this anomalous behaviour, which is unexpected in a homogeneous mixed-phase regime [11, 18], will be discussed below.

Because of demagnetisation effects the H_a versus T phase diagram depends on the sample shape [18]. Therefore we prefer to construct the H versus T diagram, where $H =$

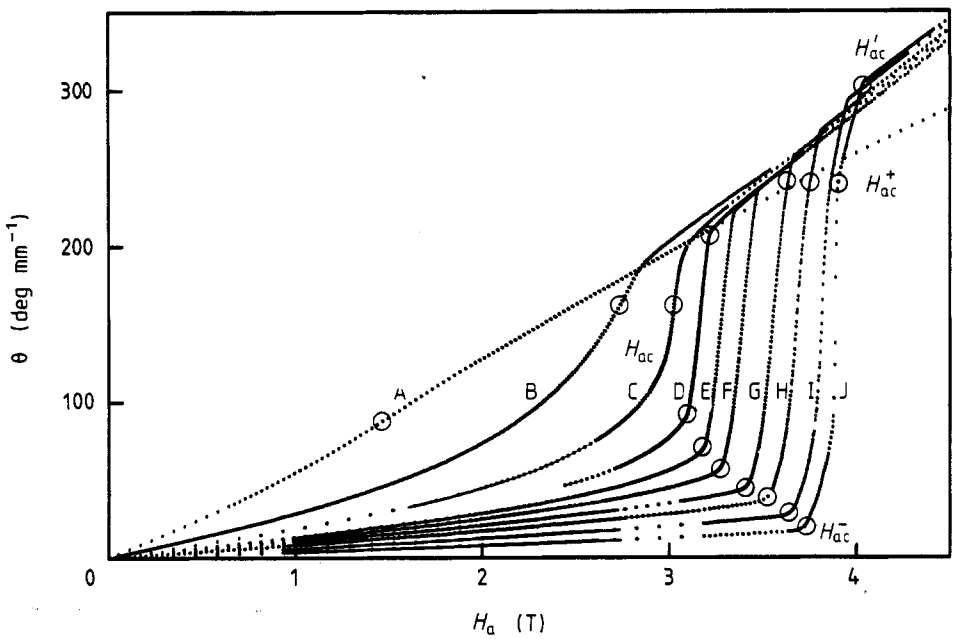

Figure 2. θ versus H_a measured at various temperatures T in the range 40 K $\geqslant T \geqslant$ 5 K: curve A, 40 K; curve B, 35 K; curve C, 30.5 K; curve D, 27.5 K; curve E, 25 K; curve F, 22.7 K; curve G, 18.7 K; curve H, 15 K; curve I, 10 K; curve J, 5 K. The phase transition points are indicated by open circles and labelled H^-_{ac}, H^+_{ac} and H'_{ac} at curve J (T = 5 K; see text).

$H_a - NM$ is the internal field. The demagnetisation factor N is inversely proportional to the slope of the θ versus H_a curves in the mixed regime $H^-_{ac} \leqslant H_a \leqslant H^+_{ac}$, where H is expected to be constant [11, 18]. In fact, by putting $H = H_a - N'\theta$, we determine an effective demagnetisation factor N', which simultaneously accounts for the proportionality between θ and M. Estimates for pure $FeCl_2$ have shown the proportionality factor to be independent of the temperature within an error of less than 5% [18]. Hence, our value $N' = (8.17 \pm 0.03) \times 10^{-4}$ T deg mm^{-1}, as determined from the near-tricritical curve D in figure 2 by a least-squares procedure, is assumed to apply to *all* our magnetisation curves with possible systematic errors up to 5%.

Figure 3 shows some of the corrected isothermal magnetisation curves of θ versus H, at temperatures 34.2 K $\geqslant T \geqslant$ 5 K (curves A–S). The TCP (H_t, T_t) is defined by the onset of vertical jumps due to the first-order AF-to-PM transition. By visual inspection, one easily determines that 30.0 K $\geqslant T_t \geqslant$ 28.8 K from curves H and I. Careful inspection of the derivatives $(d\theta/dH)_T$ of these and further transition curves located in this temperature range (not shown) eventually reveals the TCP coordinates $H_t = 2.97 \pm 0.05$ T and $T_t = 29.3 \pm 0.2$ K.

The range of existence of the SF phase is most clearly deduced from the finite-slope part of the transition curve within $H_c \leqslant H \leqslant H'_c$, as indicated in curve S in figure 3. The location of the upper bending point at $H_c(T)$ and its variation with temperature is indicated by open circles. Their positions refer to the H^+_{ac}-values as determined from figure 2 and corrected for demagnetisation as outlined above. We thus determine the CEP field coordinate $H_{CEP} = 3.40 \pm 0.05$ T.

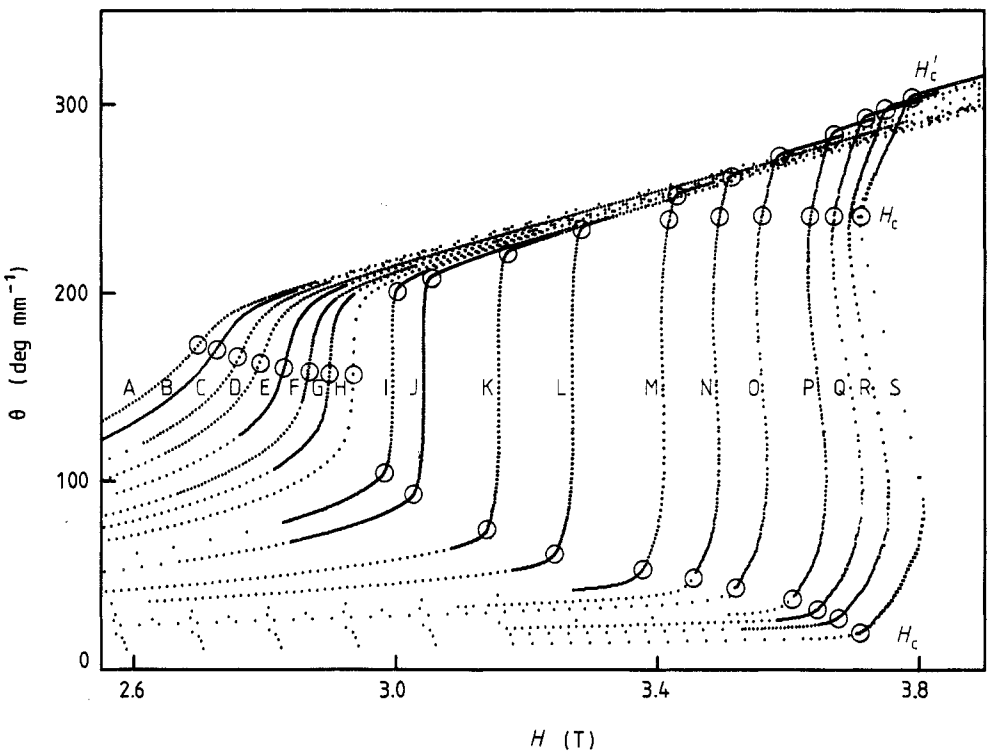

Figure 3. Internal field dependence, θ versus H, deduced from θ versus H_a data (figure 2) at various temperatures T: curve A, 34.2 K; curve B, 33.8 K; curve C, 33.1 K; curve D, 32.5 K; curve E, 31.9 K; curve F, 31.3 K; curve G, 30.5 K; curve H, 30.0 K; curve I, 28.8 K; curve J, 27.5 K; curve K, 25.0 K; curve L, 22.7 K; curve M, 19.3 K; curve N, 17.2 K; curve O, 15.0 K; curve P, 12.2 K; curve Q, 10.0 K; curve R, 8.0 K; curve S, 5.0 K. Phase transition points are indicated by open circles and labels H_c and H_c' (curve S).

As a consequence of the demagnetisation correction, the lower parts of the low-T transition curves in figure 3 become S shaped with unusual backward bending just below the AF-to-SF transition. It is noted that the upper and the lower bending points are both correctly located at the same internal phase transition field H_c. Clearly, the strange curvature of the θ versus H curves in between is determined by that of the θ versus H_a curves (figure 2) described above. Possible explanations will be given in section 4.

Figure 4 shows the complete H versus T phase diagram which contains data taken from both isomagnets (figure 1) and isotherms (figure 3), presented as open squares and open circles, respectively. It is seen that both sets of data fit well into the same scheme, where those originating from isomagnets (isotherms) are more numerous and reliable at higher (lower) temperatures as outlined above. The demagnetised phase diagram in figure 4 is continuous at the TCP (arrow), as expected. On the other hand, the CEP (arrow) does indicate a splitting of the phase boundary. In the full-scale presentation of figure 4 this is, however, barely visible. It becomes clearer in the magnified plot in the inset, where the AF–SF and SF–PM phase lines are seen to intersect at a fairly acute angle. As mentioned above, this makes an exact determination of the CEP coordinates difficult.

A more drastic visualisation of the phase transition scheme is given by the θ versus T phase diagram shown in figure 5. Here, the magnetisation values appearing at the

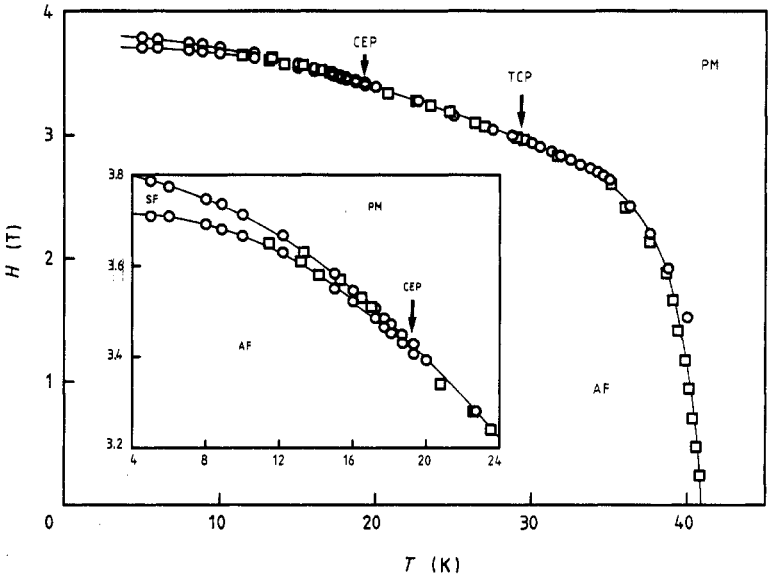

Figure 4. H versus T phase diagram of $Fe_{0.5}Ni_{0.5}Cl_2$ as determined from magnetisation isomagnets (□) and isotherms (○). The phase boundary is continuous at the TCP (arrow), but splits at the CEP (arrow; see also magnified plot in inset). The data points are interpolated by eye-guiding lines.

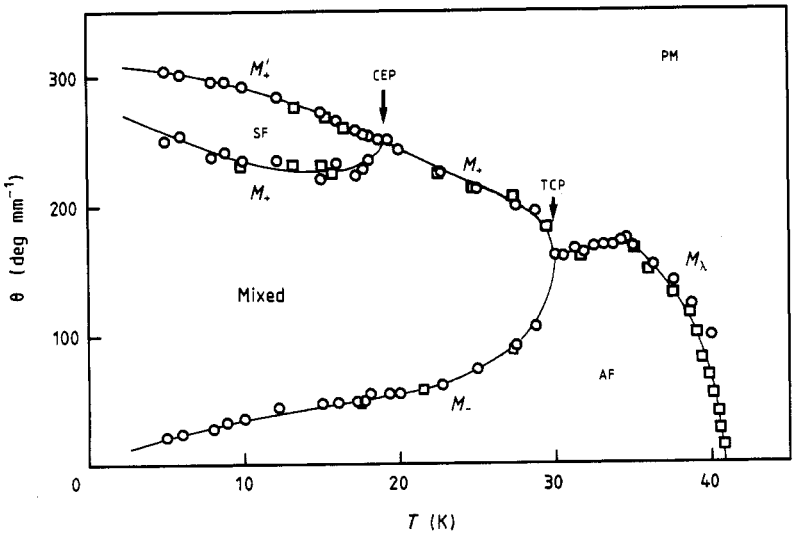

Figure 5. θ versus T diagram of $Fe_{0.5}Ni_{0.5}Cl_2$ corresponding to the data points of the H versus T phase diagram in figure 4. The eye-guiding lines M_+, M_- and M_λ meet at the TCP (arrow), whereas M_+ and M'_+ join at the CEP (arrow). The stability ranges of the AF, PM, SF and mixed phases are indicated (see text).

respective phase boundaries are plotted [18]. Within $T_t \leqslant T \leqslant T_N$ the second-order character of the M_λ line is clearly seen, whereas a very distinct splitting into the lines M_- and M_+ arises below T_t. The M_λ versus T curve has a maximum above T_t, at $T \approx 34$ K, which has carefully been checked to be real. This contrasts with the monotonic behaviour of M_λ lines in pure Ising systems and in mean field (MF) models of weakly anisotropic systems [8]. Moreover, the apparently non-linear variation in $M_+ - M_-$ with T as $T \rightarrow T_t$ seems to contradict theoretical predictions [4] which, however, may not apply to the present random system owing to its upper marginal dimension $D > 3$ at the TCP. Future, more careful studies are needed in order to decide whether the range of linearity is drastically reduced in intermediate-anisotropy systems or whether the observed non-linearity is artificially due to erroneous data evaluation. Indeed, as will be discussed below, serious errors in determining the first-order phase boundaries may arise because of non-uniform demagnetisation in our non-ellipsoidal sample. Moreover, effects due to unavoidable concentration gradients have to be taken into account. Small discontinuities of θ versus H or θ versus T then easily appear rounded and mask the real TCP, which would then lie above our experimental value of T_t.

The splitting of M_+ and M_- increases rapidly on lowering T. This is compatible with the usual decrease in the parallel AF susceptibility (i.e. M_-) and with the temperature-controlled increasing saturation of the PM magnetisation (i.e. M_+). Below the CEP the upper phase boundary into the PM phase obviously goes continuously from M_+ into M'_+. The AF–SF phase line M_+, on the other hand, seems to split off from the metamagnetic M_+ line. This seems to agree with the calculations to be discussed below.

4. Discussion

4.1. Magnetisation curves at low temperatures

Let us first discuss the unusual deviations of the up-scan θ versus H_a curves from linearity in the low-T transition regime $H_a \geqslant H_{ac}^-$ (figure 2). At first glance a plausible explanation might be given by the keyword 'metastability'. Indeed, at the first-order phase transition the AF phase might persist in a metastable state at increasing H_a, suppressing the nucleation of the SF phase up to just below H_{ac}^+. On the other hand, on lowering H_a, one would expect linear θ versus H_a behaviour or even deviations to *larger* θ-values. Such a behaviour was for example ascertained on pure $FeCl_2$ undergoing field cycles around the metamagnetic phase transition [19]. In the present case of $Fe_{0.5}Ni_{0.5}Cl_2$, however, the field-down sweep does not restore the expected straight connection between H_{ac}^+ and H_{ac}^-. Instead, the down-scan curve closely follows the up-scan θ versus H_a curve. Only a small hysteresis is revealed by a slight difference of both curves at low T.

The main origin of the deviations of both up- and down-scan curves from linearity is most probably due to inhomogeneous demagnetisation. Since the demagnetisation factor decreases from the axis to the rim of a cylindrical sample [20], the SF phase will appear first at the periphery when increasing H_a. Owing to its strong magnetisation the hollow cylindrical SF domain will then decrease the axial field by its demagnetisation field. By this effect the SF phase remains suppressed in the axial region unless H_a approaches H_{ac}^+ upon both increasing and decreasing the field. Experiments with differently shaped samples are in preparation in order to study the role of inhomogeneous demagnetisation.

As to the hysteresis observed, we believe that the excess magnetisation induced by the field decrease is due to pinning of differently registered AF domains. This process involves both random bonds and RF [21, 22] and was similarly observed for $Fe_{1-x}Co_xCl_2$ undergoing either PM-to-AF or SF-to-AF first-order transitions [11]. In the case of $Fe_{0.5}Ni_{0.5}Cl_2$, however, hysteresis becomes unmeasurably small at $T > 12$ K. Hence, apart from the very-low-T range, our compound seems to have the properties characteristic of broad domain wall systems with rapidly relaxing domain states, e.g. MnF_2 [22]. This interesting aspect of intermediate anisotropy will be discussed elsewhere [17].

4.2. *Phase diagrams*

It is now interesting to compare the phase diagram obtained experimentally (figure 4) with theoretical calculations. They are based on the theory published previously [8] and treat the mixed system $Fe_{0.5}Ni_{0.5}Cl_2$ in the virtual-crystal approximation, i.e. by using weighted averages of the magnetic model parameters of $FeCl_2$ [23] and $NiCl_2$ [24], both of which have an effective spin $S = 1$ at low temperatures. These are (in kelvins) the exchange constants with six nearest and six next-nearest in-plane neighbour spins, $J_1 = 3.94$ (21.70) and $J_2 = -0.52$ (-4.85), respectively, and with six nearest out-of-plane neighbours, $J_1' = -0.18$ (-0.77), and the single-ion anisotropy constants $D_1 = 9.8$ (-0.40) for $FeCl_2$ ($NiCl_2$). The average values $\bar{J}_1 = 12.82$, $\bar{J}_2 = -2.69$, $\bar{J}_1' = -0.48$ and $\bar{D}_1 = 4.7$ are then inserted into the two-sublattice Hamiltonian [8]

$$\chi = J' \sum_{\substack{i \neq j \\ \text{NN}}} \boldsymbol{S}_i \cdot \boldsymbol{S}_j - J \sum_{\substack{k \neq 1 \\ \text{NNN}}} \boldsymbol{S}_k \cdot \boldsymbol{S}_1 - D \sum_i (S_i^z)^2 - H \sum_i S_i^z \tag{1}$$

by putting $J' = -\bar{J}_1'$ and $J = (\bar{J}_1 + \bar{J}_2)/2 = 5.07$. Here J' determines the inter-sublattice AF interaction with $z' = 6$ neighbours, whereas J stands for the effective ferromagnetic intra-sublattice interaction with $z = 12$ nearest and next-nearest neighbours. $D = \bar{D}_1$ describes the effective single-ion anisotropy, and the axial field H determines the Zeeman energy. The multicritical behaviour of the system is now determined, in the approximation used in [8], i.e. for spin-1 systems treating D exactly and J and J' within the mean-field approximation. The parameter values $E = z'J' = 2.88$, $E_1 = zJ/2 = 30.42$ and $D = 4.7$ or, in reduced units, $e = 1$, $e_1 = E_1/E = 10.56$ and $d = D/E = 1.63$ have been used. It should be noted that these parameters do not change essentially, if only nearest-neighbour interactions were taken into account when mapping the spin Hamiltonian of the rhombohedral layered compounds $FeCl_2$ and $NiCl_2$ onto the two-sublattice model system [8]. By neglecting $\bar{J}_2$ and putting $z = 6$, one then obtains $e = 1$, $e_1' = 13.35$ and $d = 1.63$.

Calculations with the original set of parameters (e, e_1, d) yield a somewhat disappointing result (not shown). In the H–T plane, one merely obtains a TCP at $T_t \approx 0.97 T_N$, below which the thermodynamic first-order phase transition line extends down to $T = 0$ without any hint of an additional SF phase. We believe this to be due to a misbalance of the different approximations involved in the calculation. Clearly, the uniaxial anisotropy, which is correctly treated, will be overemphasised in comparison with the exchange interaction, accounted for in the mean-field approximation. It is then reasonable to reduce the ratio $d = D/E$ in order to obtain a consistent result. Indeed, upon letting $d < 1$ the desired SF phase emerges similarly as observed experimentally. It separates the AF from the PM phase between $T = 0$ and the CEP, which finally merges into the TCP at $d \approx 0.31$, where $T_t = 14.61$ and $H_t = 0.209$.

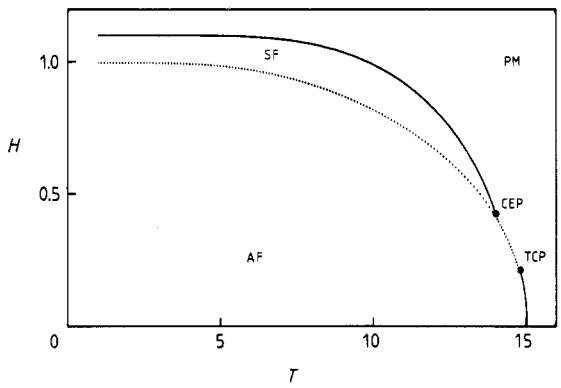

Figure 6. Phase diagram H versus T in units of $E = z'J'$ calculated for $D/E = 0.90$ and $E_1/E \equiv 10.56$: ———, second-order transitions; . . . . , thermodynamic critical fields of first-order transitions. TCP and CEP are the tricritical point and the critical end point on the transition lines PM to AF and SF, respectively.

Figure 6 shows the H–T phase diagram, which appears to be closest to the experimental phase diagram (figure 4). It refers to the parameters $e_1 = 10.56$ and $d = 0.9$ and exhibits a narrow range of stability of a low-T SF phase up to $T_{CEP} = 0.93T_N$, and a first-order phase transition line, PM–AF, between T_{CEP} and $T_t = 0.98T_N$. Obviously, a similar situation is encountered as in the experiment (figure 4), where, however, the TCP is found at substantially lower temperatures, $T_t = 0.72T_N$. In order to simulate this condition the ferromagnetic exchange parameter might be reduced. This was shown by the phase diagram in figure 4 of [8], which comes very close to the experimental phase diagrams with the parameters $e_1 = 0.4$ and $d = 0.9$. Such a set of parameters is, however, unrealistic to apply to any mixture of $FeCl_2$ and $NiCl_2$. Both of these layered compounds have predominant ferromagnetic intra-planar exchange, which inevitably yields $e_1 > 1$ at any rate. Presumably the virtual-crystal approximation, which completely neglects the randomness of the system, induces systematic errors. It will be interesting to include effects of randomness, and in particular randomness of the crystal-field anisotropy D, also in our present calculations on anisotropic antiferromagnets.

5. Conclusions

$Fe_{0.5}Ni_{0.5}Cl_2$ has been shown to come close to a Heisenberg antiferromagnet with intermediate uniaxial anisotropy. This is evidenced by M versus H and M versus T measurements using Faraday rotation. H versus T and M versus T phase diagrams constructed from these data exhibit a low-T SF phase, placed above the conventional first-order phase boundary of the AF phase. Its CEP lies close to the TCP.

Experiments are currently under way to study systems with different concentrations in order to observe the theoretical [8, 9] predicted shift of the CEP towards the TCP. It will be interesting to study the properties of the NMP, where the CEP and the TCP coalesce. Clearly, the present ambiguities in determining exactly the multicritical points have to be remedied. Care has to be taken to avoid both concentration gradients and inhomogeneous demagnetisation. Moreover, future theoretical considerations should include the effects of the random anisotropy. The present discrepancies between measured and calculated H versus T phase diagrams are very likely to be due to the virtual-crystal approximation, assuming average single-ion anisotropy constants.

Acknowledgments

Thanks are due to W Nitsche for technical advice and to H Junge for the crystal growth. This work was supported through Sonderforschungsbereich 166 by the Deutsche Forschungsgemeinschaft.

References

[1] Néel L 1932 *Ann. Phys., Paris* **18** 5
[2] Rohrer H 1975 *Phys. Rev. Lett.* **34** 1638
[3] Wolf W P 1977 *Physica* B **86–8** 550
[4] Lawrie I D and Sarbach S 1984 *Phase Transitions and Critical Phenomena* vol 9, ed J L Lebowitz (London: Academic) p 50
[5] Fisher M E 1975 *Phys. Rev. Lett.* **34** 1634
[6] Griffin J A, Litster J D and Linz A 1977 *Phys. Rev. Lett.* **38** 251
[7] Gorter C J and Peski-Tinbergen T V 1956 *Physica* **22** 273
[8] Vilfan I and Galam S 1986 *Phys. Rev.* B **34** 6428
[9] Galam S and Aharony A 1980 *J. Phys. C: Solid State Phys.* **13** 1065
[10] Wong P Z and Cable J W 1984 *Phys. Rev.* B **30** 485
Wong P Z 1986 *Phys. Rev.* B **34** 1864
[11] Nitsche W and Kleemann W 1988 *Phys. Rev.* B **37** 7680
[12] Ito A, Torikai E, Kitazawa M, Tamaki T, Goto T, Sakakibara T, Todo S and Oguro I 1986 *J. Magn. Magn. Mater.* **54–7** 39
[13] Ito A, Tamaki T, Someya Y and Ikeda H 1983 *Physica* B **120** 207
[14] de Gunzbourg J, Papassimacopoulus S, Miedan-Gros A and Allain Y 1971 *J. Physique* **32** C1 125
[15] Leitão U A and Kleemann W 1987 *Phys. Rev.* B **35** 8696
[16] Kleemann W, King A R and Jaccarino V 1986 *Phys. Rev.* B **34** 479
[17] Igel B 1989 *Diplomarbeit* Duisburg Universität
[18] Dillon J F, Chen E Y and Guggenheim H J 1978 *Phys. Rev.* B **18** 377
[19] Chen E Y, Dillon J F Jr and Guggenheim H J 1974 *Magnetism and Magnetic Material (AIP Conf. Proc. 24)* (New York: American Institute of Physics) p 200
[20] Joseph R I and Schlömann E 1965 *J. Appl. Phys.* **36** 1579
Brug J A and Wolf W P 1985 *J. Appl. Phys.* **57** 4685
[21] Leitão U A, Kleemann W and Ferreira I B 1988 *Phys. Rev.* B **38** 4765
Pollak P, Kleemann W and Belanger D P 1988 *Phys. Rev.* B **38** 4773
[22] Nattermann T and Vilfan I 1988 *Phys. Rev. Lett.* **61** 223
[23] Birgeneau R J, Yelon W B, Cohen E and Makovsky J 1972 *Phys. Rev.* B **5** 2607
Wiltshire M C K and Hayes W 1978 *J. Phys. C: Solid State Phys.* **11** 3701
[24] Lindgård P A, Birgeneau R J, Als-Nielsen J and Guggenheim H J 1975 *J. Phys. C: Solid State Phys.* **8** 1059